Geophysical Journal International

Geophys. J. Int. (2010) **183,** 1633–1647 doi: 10.1111/j.1365-246X.2010.04818.x

Numerical modelling of ground motion in the Taipei Basin: basin and source effects

J. Miksat[1], K.-L. Wen[2], F. Wenzel[1], V. Sokolov[1] and C.-T. Chen[2]

[1] *Geophysical Institute, Karlsruhe Institute of Technology, Karlsruhe, Germany. E-mail: joachim.miksat@kit.edu*
[2] *Institute of Geophysics, National Central University, Jongli City, Taiwan*

Accepted 2010 September 19. Received 2010 September 7; in original form 2009 October 13

SUMMARY

The Taipei basin in northern Taiwan is located in a high seismicity region and was affected by several earthquakes in the past ($M_L = 7.3$ on 1909 April 15; $M_L = 6.8$ on 1986 November 15; the Chi-Chi $M_L = 7.3$ earthquake on 1999 September 21 and $M_L = 6.8$ on 2002 March 31). The main characteristic of the Taipei basin is its complex shape with a deep western and shallow eastern part. The uppermost Sungshan formation with its low shear wave velocities (90–200 m s^{-1}) is also a distinct feature of the basin. Based on the large data base of earthquake records obtained from the Taiwan Strong Motion Instrumentation Program network, many studies on ground motion within the Taipei basin exist. However, the influence of the various subsurface structures on the observed ground motions as well as the variability of ground motion with respect to earthquake location is not fully understood. We apply a 3-D finite-difference method to simulate wave propagation up to 1 Hz for a small earthquake close to the basin in order to resolve these open questions. By varying source and structural parameters, we explore the variability of ground motion.

Our study includes a subsurface model that is based on recent studies on the basin structure and on the crustal structure of Taiwan. From our simulations we find a good fit between simulated and observed waveforms and peak ground accelerations for the considered small earthquake near the basin. We also explore the influence of fault plane orientation, hypocentre location, deep basin structure and soft soil surface layers of the Sungshan formation by varying the subsurface structure and earthquake position. Our studies reveal that the basin structure produces an amplification factor of about 4 compared to hard rock conditions. Additionally, the soft soil Sungshan formation produce amplification of a factor of 2. This results in a maximum amplification of the basin structure of about 8, which is in good comparison with amplification values larger than 5 found from the analysis of observed earthquakes. These values clearly exceed the amplification values of about 2–3 obtained when applying standard 1-D site effect analysis.

Our simulations for different earthquake positions show that ground motion depends strongly on earthquake location and fault orientation. Therefore, the application of average values of spectral amplification obtained from the analysis of recorded data from distant earthquakes with different azimuths and fault planes may significantly underestimate future ground motions of possible earthquakes on known faults close to the Taipei basin. The simulation of a small earthquake near the Taipei basin presented in this study will help to set up adequate simulation parameters for a possible large earthquake close to the Taipei basin. Such a simulation of a scenario earthquake close to the Taipei basin would allow to significantly improve hazard assessment as no observations of strong earthquakes in the vicinity of the basin exist.

Key words: Earthquake ground motions; Site effects; Computational seismology; Wave propagation.

1 INTRODUCTION

The city of Taipei in northern Taiwan with a population of about 3 millions is located on a complex shaped sedimentary basin. The city suffered last century four times from strong earthquakes ($M_L = 7.3$ on 1999 April 15; $M_L = 6.8$ on 1986 November 15; the Chi-Chi $M_L = 7.3$ earthquake on 1999 September 21 and $M_L = 6.8$ on 2002 March 31). The Taipei basin can be divided into a deep

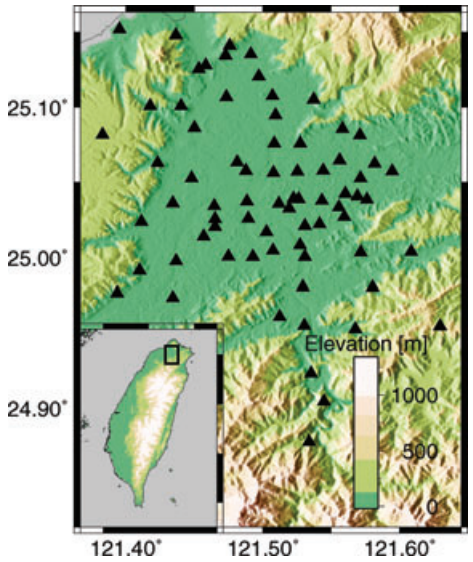

Figure 1. Map of the triangle-shaped Taipei basin in northern Taiwan. The area is covered with a dense strong motion network (triangles), which is operated within the frame of the Taiwan Strong Motion Instrumentation Program (TSMIP).

western (750 m) and a more shallow eastern part (200–300 m). The uppermost sedimentary layer is the so-called Sungshan formation with minimum shear wave velocities of about 100 m s^{-1}. A deep understanding of site amplification within the complex shaped Taipei basin is essential for seismic hazard assessment.

The Taipei area is covered with a dense strong motion network (Fig. 1) that is operated within the frame of the Taiwan Strong Motion Instrumentation Program (TSMIP) conducted by the Central Weather Bureau (CWB). Many studies of recorded events exist that describe ground motion patterns within the basin (e.g. Wen & Peng 1998; Sokolov *et al.* 2000, 2003, 2004; Chen 2003; Fletcher & Wen 2005). These studies revealed a large variation of ground motion characteristics like peak ground acceleration, response spectra, and dominant frequencies in the Taipei basin.

More recently, frequency dependent site amplifications were derived by application of the so-called 'very hard rock' (VHR) spectral model (Sokolov *et al.* 2009). This analysis included records at 32 stations from 83 deep and 142 shallow earthquakes. The results showed that for shallow earthquakes strong surface waves are produced within the basin. In some cases shallow earthquakes produce high amplifications for frequencies from 0.3 to 1 Hz which may be dangerous for high-rise buildings and highway bridges. Chen *et al.* (2009, personal communication) applied the H/V method in order to explore spectral amplifications of deep and shallow earthquakes from different azimuths. They found also strong low frequency (f < 2–3 Hz) amplifications for shallow earthquakes with clear earthquake azimuth dependence at some stations. All these studies allow a detailed description of site amplification within the basin. However, the influence of earthquake location, fault orientation and of the different subsurface features cannot be fully separated by these methods.

By applying numerical modelling of wave propagation, these open questions can be addressed. The comparison between simulations for different subsurface structures and different source properties allow to assess their influence on ground motions. Various numerical simulations have been performed in the past to explore ground motions in the Taipei basin. These simulations revealed that the complex basin structure produces distinct wave propagation patterns. Lee *et al.* (2008a) applied a composite finite-difference method to simulate 3-D amplification effects within the basin and found the important influence of basin geometry and the low velocity Sungshan formation on the resulting ground motions by evaluating simulation results along a profile through the basin. Lee *et al.* (2008b) applied a spectral element method (SEM) to simulate ground motions for the Taipei basin. This study also revealed the strong influence of basin depth and the Sungshan formation on ground motions within the basin. Both studies (Lee *et al.* 2008a,b) also revealed the generation of strong surface waves within the basin. Lee *et al.* (2009) found that for distant earthquakes mountain ranges on the wave path may play an important role for ground motion amplitude in the basin. Miksat *et al.* (2009) studied site amplification by simulating planar wave front incidence on the Taipei basin by applying a 3-D finite-difference method. They found that shallow earthquakes produce strong surface waves compared to deep scenarios and showed qualitatively that numerical modelling is capable to calculate frequency dependent site amplifications for the Taipei basin.

In this study, we aim at a more detailed analysis of the influence of the subsurface structure with a special emphasis on the dependence of ground motions on earthquake location and fault plane solution. In addition, compared to former works, we utilize in this study an improved subsurface model that includes recent data on the crustal and mantle structure of Taiwan obtained from seismic tomography (Wu *et al.* 2007). We apply a 3-D finite-difference (FD) code to explore wave propagation (Furumura & Kennett 2005). Our study starts with the simulation of the 2004 October 23 $M_L = 3.8$ earthquake that occurred in the vicinity of the basin. This is the only shallow earthquake that occurred in the vicinity of the basin with magnitude larger 3.5, with an available high quality fault plane solution and that was recorded by numerous stations. We validate our modelling by comparing observed and simulated ground motions of this event. Next we focus on a detailed description of the source and basin effects on ground motion within the basin by variations of source position and subsurface structure and estimate the variability of ground motions. Furthermore, we compare our calculated spectral amplifications with standard 1-D analysis of site amplification. Compared to 1-D analysis of site effects our numerical simulations include also 3-D effects due to the basin structure as well as basin induced surface waves which allows a more reliable site amplification estimation for complicated subsurface structures. Because of the model size and the dense spatial sampling high performance computing (HPC) is absolutely necessary. In order to perform efficient simulations a hybrid MPI/OpenMP approach is applied.

2 TAIPEI BASIN MODEL

After a stage of mountain uplift in the area that is now covered by the Taipei city, extension started influenced by large scale regional tectonics. The Tertiary basin was formed by subsidence starting 0.4 Ma ago along the Sanchiao fault, which is marked by the northwest border of the basin (Teng *et al.* 2001). Then the basin was filled by alluvium deposits, which resulted in flat-lying Quaternary layers. A detailed structure of the basin was obtained by seismic reflection profiles through the city and geotechnical drilling (Wang *et al.* 2004). Wang *et al.* (2004) gives the depths of the Tertiary basin and structural information on the sedimentary layers within the basin. We combine the SRTM Shuttle Radar Topography Mission (CIAT 2004) and the basin depth (Wang *et al.* 2004) and created a basin-topography layer shown in Fig. 2. The uppermost layer of

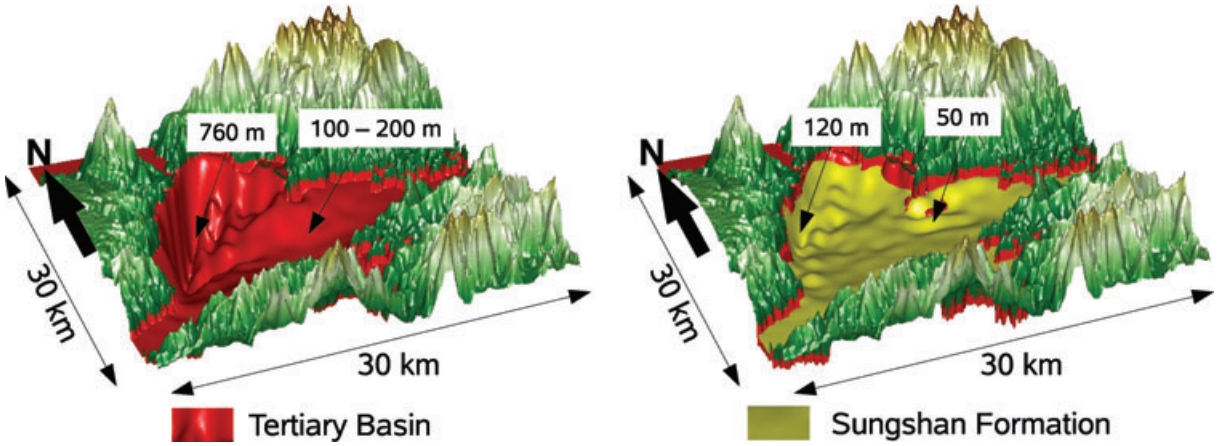

Figure 2. Left-hand panel: topography and tertiary basement depth (red layer). The Taipei basin can be divided into a deep western (760 m) and a shallow eastern part (200–300 m). Right-hand panel: the depth of the uppermost soft soil layer, the Sungshan formation, is indicated by the yellow surface. Maximum depth is about 120 m in the western part of the basin and about 50 m in the eastern part.

the sediments the so-called Sungshan formation is represented by very low shear wave velocities (90–200 m s^{-1}). We embedded the Taipei basin structure into the subsurface model derived by Wu *et al.* (2007) from seismic tomography.

To describe the sedimentary layering within the basin, we take average seismic velocities of the sediments given by Wang *et al.* (2004) in a table on page 622 of their paper. In this case constant minimum shear wave velocity at the surface is 170 m s^{-1}. From the average seismic velocities given by Wang *et al.* (2004) velocity–depth functions are developed for the Sungshan formation and the deeper sedimentary layers. The applied relations for the depth dependence of v_P and v_S velocities of the Sungshan formation are

$$v_p^{\mathrm{Sun}}(d) = -1.15\ \mathrm{km\,s^{-1}} \left(\frac{0.1\ \mathrm{km} - |d|}{0.1\ \mathrm{km}}\right)^4 + 1.6\ \mathrm{km\,s^{-1}},$$

and

$$v_s(d)^{\mathrm{Sun}} = 0.17\ \mathrm{km\,s^{-1}} \left(\frac{|d|}{0.3\ \mathrm{km}}\right) + 0.17\ \mathrm{km\,s^{-1}}. \quad (1)$$

Here, d is depth in km. For the sedimentary layers beneath the Sungshan formation and beneath the earth surface we apply

$$v_p^{\mathrm{Sed}}(d,x,y) = 0.4\ \mathrm{km\,s^{-1}} \left[\frac{|d| - |d_{\mathrm{Sun}}(x,y)|}{0.7\ \mathrm{km} + |d_{\mathrm{Sun}}(x,y)|}\right]^{0.6} + 1.8\ \mathrm{km\,s^{-1}},$$

and

$$v_s^{\mathrm{Sed}}(d,x,y) = (0.43\ \mathrm{km\,s^{-1}}) \left[\frac{|d| - |d_{\mathrm{Sun}}(x,y)|}{0.7\ \mathrm{km} + |d_{\mathrm{Sun}}(x,y)|}\right]^{0.75} + 0.45\ \mathrm{km\,s^{-1}}, \quad (2)$$

where d is depth in km and $d_{\mathrm{Sun}}(x, y)$ is the depth of the Sungshan formation at the corresponding EW and NS distances x and y in km from the origin of the model at 121.3665°N, 24.91064°E.

For depths greater than the Tertiary basin, we adopt a recent published velocity structure for the Taiwan area by Wu *et al.* (2007) derived from seismic tomography. They utilized 41 141 S-P times from records of 680 stations of the TSMIP network. Density needed for FD simulation is calculated from *P*-wave velocities after Glaznev *et al.* (1996). In order to obtain the velocity and density values at the gridpoints of the FD grid, a Matlab triangle-based cubic interpolation routine is applied.

To examine the influence of the subsurface structure on the ground motions within the Taipei basin, we also apply some subsurface structures different from the here described one. Details on these models are given when utilized in the subsequent sections.

3 2004 OCTOBER 23 EARTHQUAKE

On 2004 October 23, a $M_{\mathrm{L}} = 3.8$ earthquake occurred beneath the Taipei basin (Fig. 3). It was the largest event close to the Taipei basin during the last years with an available accurate fault plane solution. Due to its vicinity to the basin and the shallow depth of about 9 km, we assume that the influence of the Taipei basin structure is much more important compared to the influence of the path between the hypocentre and the basin. Therefore, this event should be useful to study the basins influence on ground motion. Additionally, the small magnitude corresponds to a small fault size and a simple source time function in the low frequency range. However, it was strong enough to trigger many stations of the TAP TSMIP network. Consequently, this earthquake is very suitable for comparison of observation and

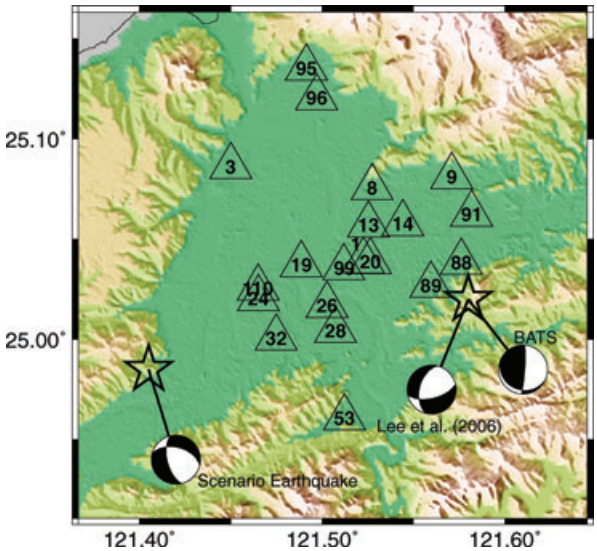

Figure 3. Map of the Taipei basin with fault plane solutions of the 2004 earthquake after Lee *et al.* (2008a) and the BATS catalogue. We also evaluate a scenario earthquake near the SW edge of the basin.

modelling results. Therefore, in this paper we first compare simulated and observed ground motions of this event for our developed Taipei basin model (see Section 2). Then we study the influence of the different subsurface structures by alternating the model. In order to examine the influence of source radiation, we simulate wave propagation for two different fault plane solutions. One fault plane solution was found from an inversion study performed by Lee *et al.* (2006) and referenced in Lee *et al.* (2008b). Another solution is published in the Broadband Array in Taiwan for Seismology (BATS) CMT catalogue (http://bats.earth.sinica.edu.tw/). The fault parameters of both solutions are listed in Table 2. Fig. 3 displays fault plane solutions for both events.

4 NUMERICAL MODELLING

We use a 3-D FD method (Furumura & Chen 2005; Furumura & Kennett 2005) for wave propagation simulations. The spatial derivatives of the equations are calculated by a high-order 16th FD scheme in horizontal directions x and y and a low-order 4th scheme in vertical direction z with a half grid interval ($dz = 1/2dx$; $dz = 1/2dy$) on a standard staggered grid (Madariaga 1976). The high-order FD method offers a good accuracy and low numerical dispersion even when using large grid sizes compared to lower-order FD schemes. However, the higher-order FD scheme makes seismic wavefields and material interfaces smooth. Usually heterogeneities in the crustal structure are much stronger in vertical direction and therefore the 16th/4th scheme was chosen as a balance (Furumura & Chen 2005). For a more detailed study on the influence of the position of material interfaces, see Moczo *et al.* (2002). Three gridpoints per minimum wavelength in horizontal and six gridpoints per minimum wavelength in vertical direction are required in order to obtain reliable results (Furumura & Chen 2004). Temporal accuracy of the operators is of second order. Damping (Cerjan *et al.* 1985) and one-way absorbing (Clayton & Enquist 1977) boundary conditions are applied at the sides and the bottom of the model. A flat free surface is implemented by zero stress conditions (Graves 1996). Parallelization of the simulations can be realized by domain decomposition, which is done by dividing the model into horizontal slices. Communication between the domains is done by Message Passing Interface (MPI). Each horizontal slice is assigned to one computing node. Additionally, the calculations within each node are distributed on the processors of the node by applying OpenMP. The simulations are performed on the HPXC6000 supercomputer of the Scientific Supercomputing Center Karlsruhe. We run the code on computing nodes with two Intel Itanium2 1.5 GHz processors. By adding OpenMP routines for each domain on the two processor nodes, we reach a speed up between 30 and 40 per cent compared to purely MPI usage.

The horizontal model size is 29.8 × 29.8 km. The vertical extension of the model is 16.3 km. Grid spacing is 50 and 25 m in horizontal and vertical direction, respectively. All spatial and temporal modelling parameters are listed in Table 1. The source is implemented by adding the stress glut (Olsen *et al.* 2006; Miksat *et al.* 2008) to the source gridpoint. The source time function of the added stresses for the considered $M_L = 3.8$ earthquake is described by a Herrman window with a half width of 0.5 s. The moment magnitude, which is needed to calculate the stress glut, is obtained from local magnitude by the empirical relationship of Lin & Lee (2008) for earthquakes in Taiwan.

Based on the minimum shear wave velocity of 170 m s^{-1} and grid spacing, maximum frequency of our simulations is 1 Hz. Attenuation is implemented by adopting the method proposed by Blanch *et al.* (1995). Approximate Q_S and Q_P values are calculated from the S-wave velocities by $Q_S = 0.1\, v_S$ and $Q_P = 1.5\, Q_S$, whereas v_S is used in m s^{-1}. These values are estimated because accurate values are not available. However, for the studied earthquakes in the vicinity of the basin the resulting amplitudes are not so sensitive to changes of the Q values (Lee *et al.* 2008b).

Table 1. Modelling parameters.

Horizontal discretization (m)	50
Vertical discretization (m)	25
Number of gridpoints (EW-direction)	597
Number of gridpoints (NS-direction)	597
Number of gridpoints (z-direction)	656
Horizontal extension in EW-direction (km)	29.8
Horizontal extension in NS-direction (km)	29.8
Vertical extension in z-direction (km)	16.3
Temporal discretization (ms)	1.5
Number of time steps	30 000
Simulation time (s)	45

5 RESULTS

5.1 Observed and simulated ground motions

We compare observed and simulated waveforms and peak ground accelerations for the subsurface structure that is based on the average velocity model provided by (Wang *et al.* 2004, see Section 2). Observed and modelled data were filtered (0.1–1 Hz) with a second-order Butterworth bandpass filter implemented in Matlab. In Fig. 4 snapshots of the wavefield are shown. Starting from the southeastern edge shear waves enter the basin at 3 s and propagate to the West. The resulting wavefield is very complex and shows long ground motion duration in the basin. Especially, in the central part of the western deep basin structure. This was also found by Lee *et al.* (2008b). Fig. 5 displays observed and recorded velocity waveforms for eleven stations clearly within the basin. Fig. 6 shows the comparison for eight stations near the basin edges. For almost all horizontal waveforms within the basin the shape of the first 5 s is reproduced by the modelling. Also observation and modelling show similar maximum amplitudes. We found that the fit is better for stations clearly within the Taipei basin compared to stations near the basin edges and outside the basin. An exception is station TAP008 near the northern border of the basin. The discrepancies for stations near the basin edges could be explained by limited resolution of the known basin structure. As frequency content for stations near the basin edges is higher compared to stations clearly within the basin, the limited small scale knowledge of the model would produce larger discrepancies for stations near the basin edges. In general fit is also not so good for the vertical components. Partly, this can be explained by uncertainties of the polarization direction of the records (e.g. TAP053 and TAP089). However, the maximum amplitudes of the modelled and observed vertical component are similar. Remarkably, the results of wave propagation simulation by a SEM of the same earthquake (Lee *et al.* 2008b) show also mainly larger misfits for the vertical components. For future studies a quantitative analysis of the misfits between recorded and simulated seismograms could be performed in order to analyse the seismograms more deeply and give a quantitative description of the misfits. For such complex waveforms that differ in amplitude, phase and envelope, misfit criteria like Kristeková *et al.* (2009) should be applied. In Fig. 7, we compare

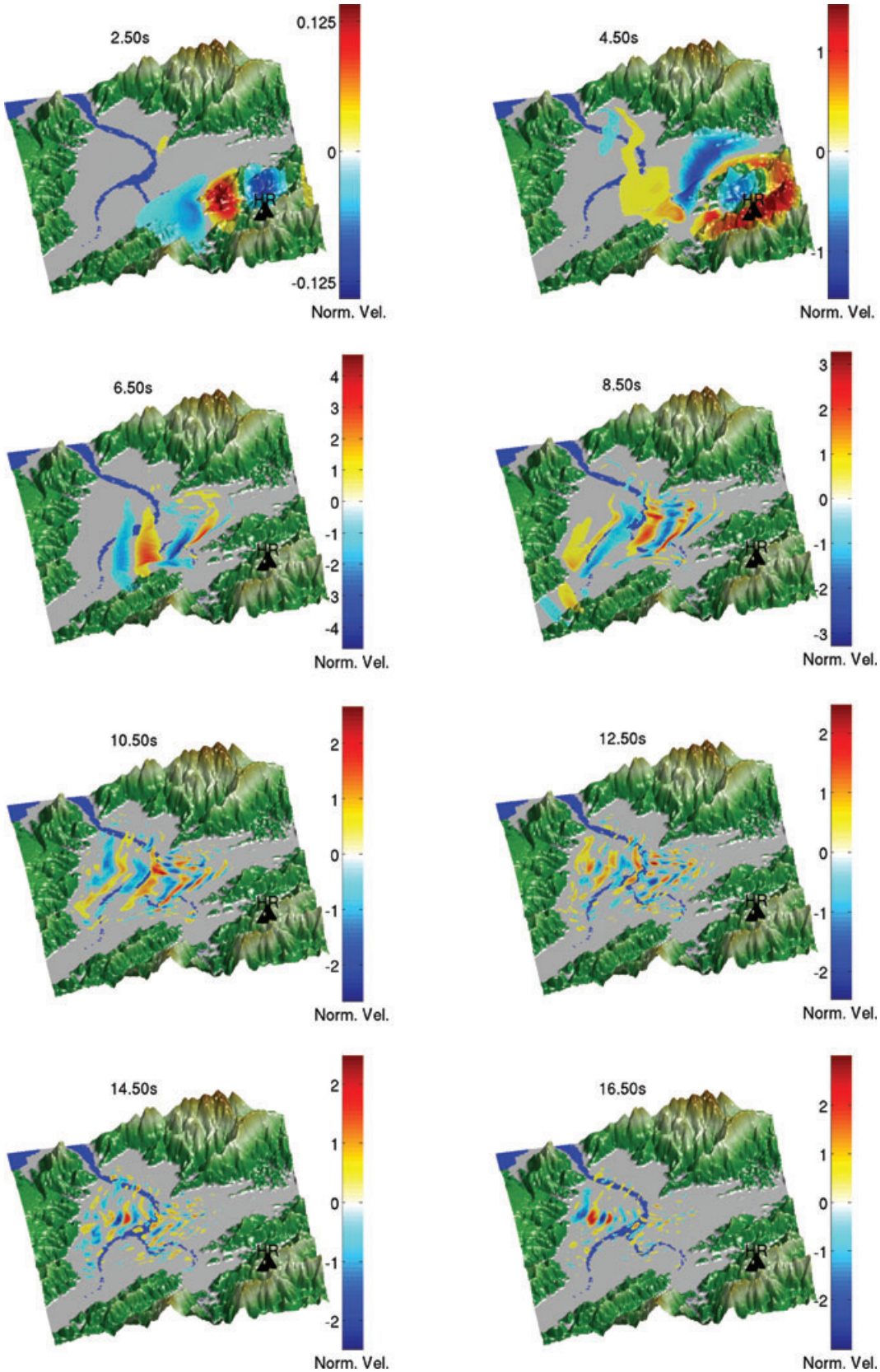

Figure 4. Snapshots of the NS-component of the modelled velocity wavefield. The colour scale gives the amplitude which is scaled to the maximum velocity at the marked hard rock (HR) station southeast of the basin. After about 3 s *S*-wave arrive at the surface and start to propagate into the basin from the SE. Surface waves are produced that travel mainly from east to west through the central part of the basin and produce a complex wavefield with long shaking in the central region of the western deep part of the basin.

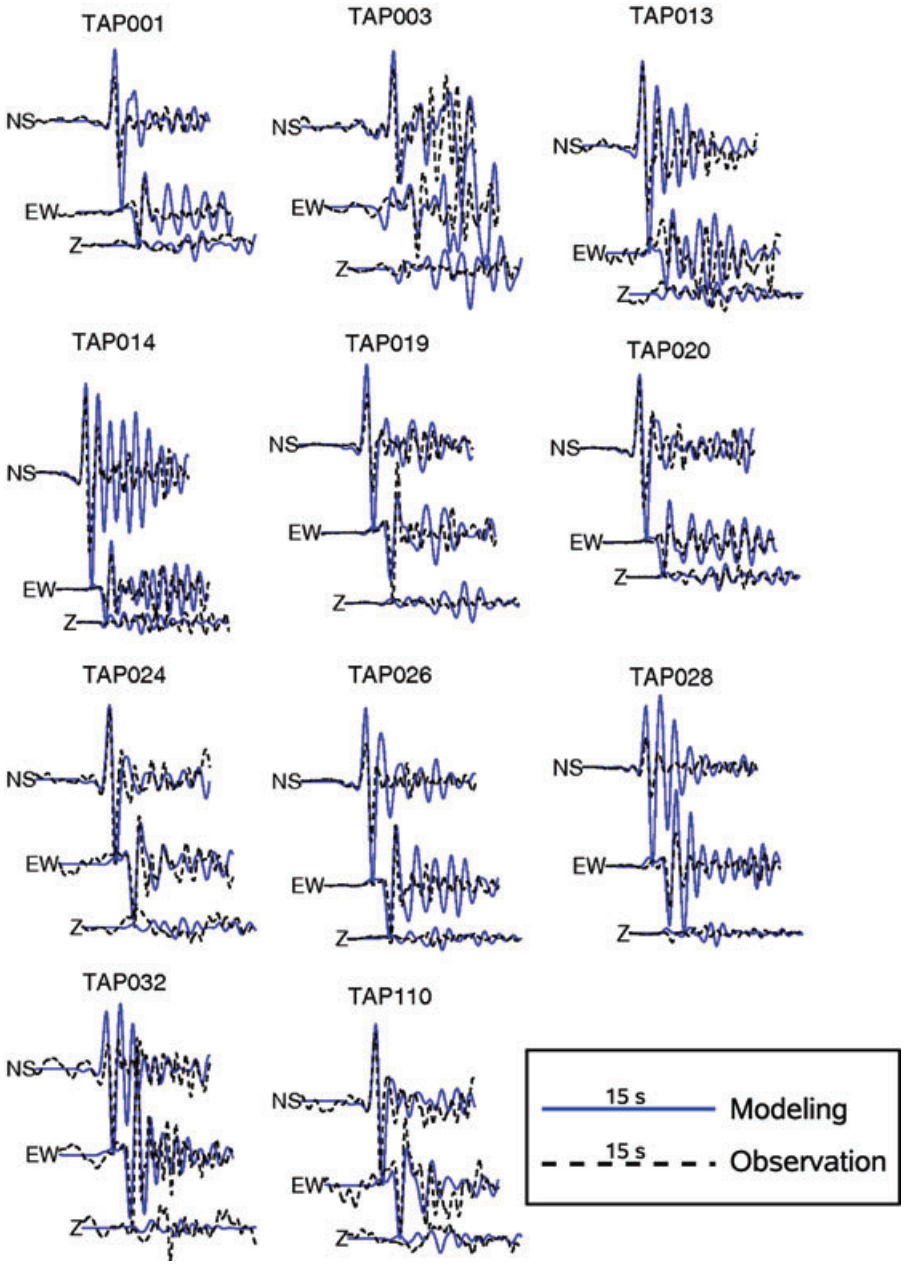

Figure 5. Comparison between observed and modelled velocity waveforms for stations within the basin of the 2004 earthquake simulated with the fault plane solution after Lee *et al.* (2006).

modelled and observed peak ground acceleration (PGA). In this paper PGA is calculated from all three components as the maximum value of acceleration $a(t) = \sqrt{a_{EW}(t)^2 + a_{NS}(t)^2 + a_v(t)^2}$. The observed distribution was interpolated from available records at stations indicated by triangles. Both PGA distribution show similar shape and maximum PGA values of about 0.8 cm s^{-2} in the considered low frequency part ($f < 1$ Hz). These results show that strong ground motion simulations for earthquakes close to the Taipei basin can produce reliable results and that the applied 3-D FD method and the utilized subsurface structure are applicable. As discussed in the introduction, it is not possible to perform another similar validation because there is not enough data on another earthquake near the basin available.

5.2 Influence of source radiation

In this section, we compare ground motions obtained from two different fault plane solutions in order to evaluate the influence of source radiation. We simulate the 2004 earthquake by utilizing fault parameters released in the BATS catalogue and compare the results with the above shown simulation that used the fault parameters after Lee *et al.* (2008b). The strike, dip and slip angles are given in Table 2. Fig. 8 shows comparison between observed and modelled seismograms at four stations. It can be seen that compared to the modelling with the fault parameters after Lee *et al.* (2006), which is shown in Fig. 5, misfit between modelled and observed amplitudes is clearly larger. Furthermore, the resulting PGA distribution (Fig. 9)

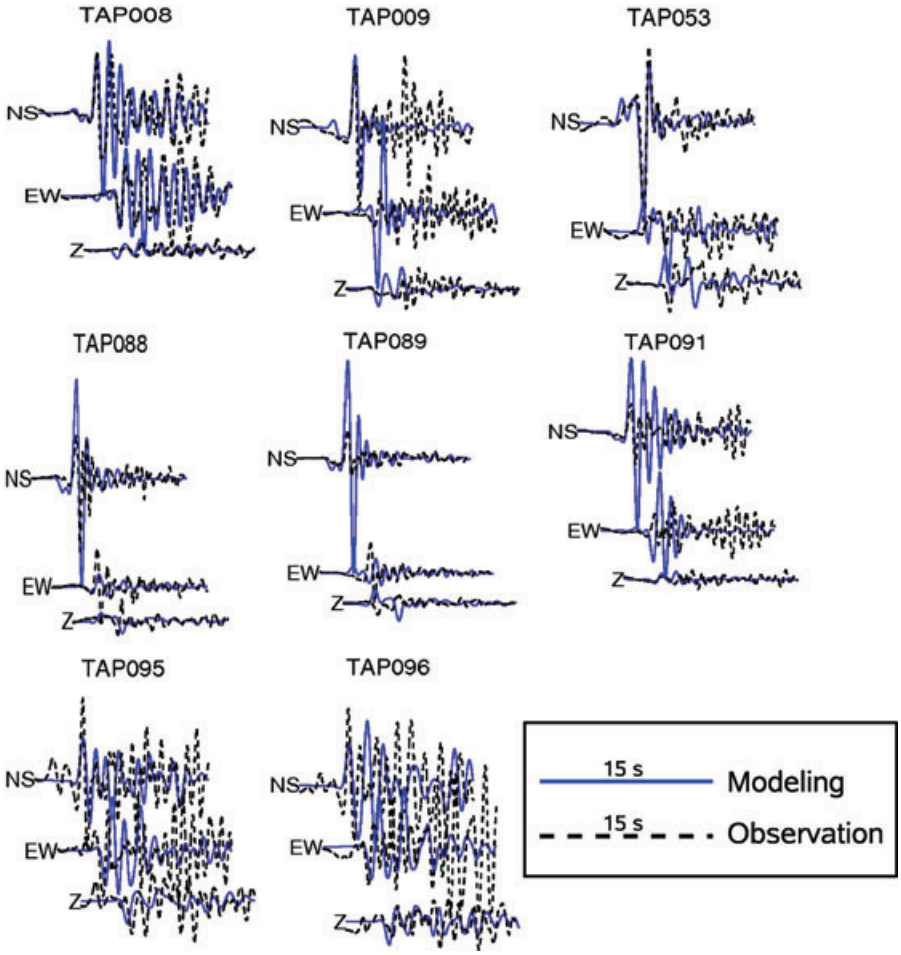

Figure 6. Comparison between observed and modelled velocity waveforms for stations near the basin edge of the 2004 earthquake simulated with the fault plane solution after Lee *et al.* (2006).

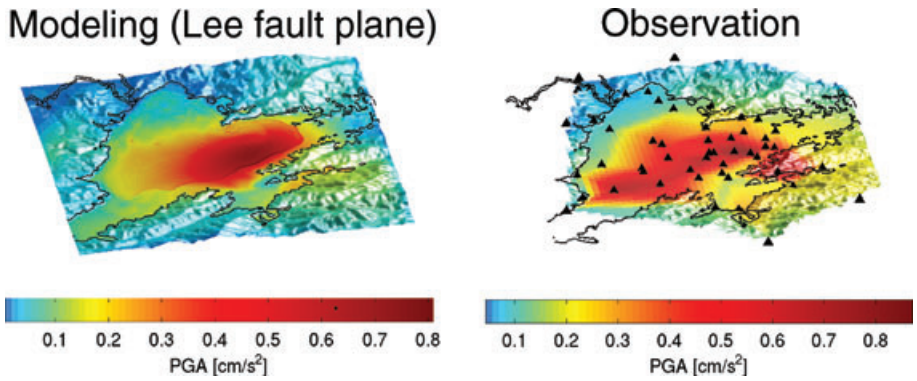

Figure 7. Comparison between observed and simulated PGA distribution of the 2004 earthquake (fault plane after Lee *et al.* 2006). The observed distribution is interpolated from the stations indicated in the figure.

Table 2. Available fault plane solutions of the 2004 October 23 earthquake.

	BATS catalogue	Lee *et al.* (2006)
Strike	3.9°	195°
Dip	84.07°	49°
Rake	106.5°	−140°

differs clearly from the PGA distribution obtained for the fault plane solution released by Lee *et al.* (2006). A NS oriented shape is obtained for the BATS fault plane solution compared to the EW oriented shape obtained by applying the solution given by Lee *et al.* (2006) and the distribution interpolated from real data (see Fig. 7). Therefore, for our further simulations in this paper, we apply Lee's fault plane solution. Furthermore, the comparison between both

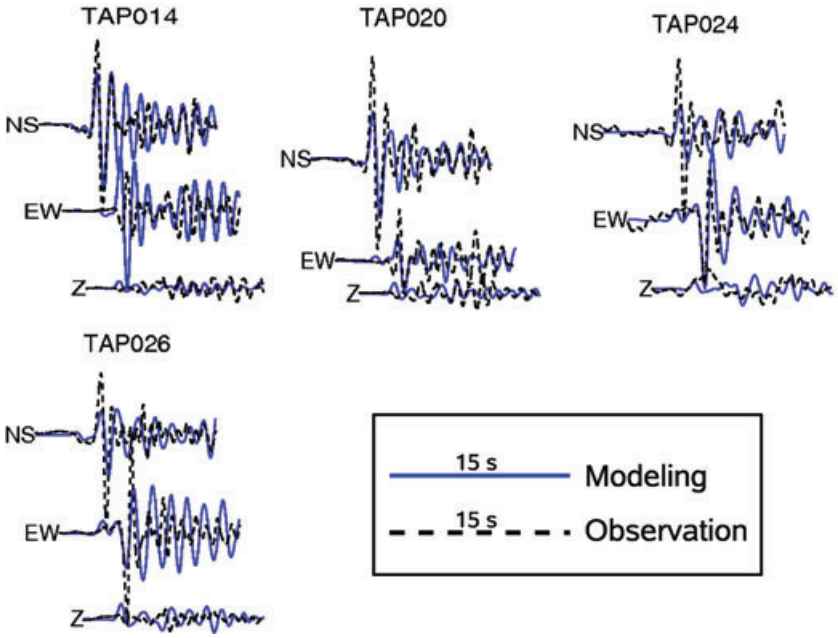

Figure 8. Comparison between observed and simulated velocity waveforms of the 2004 earthquake (fault plane after the BATS catalogue).

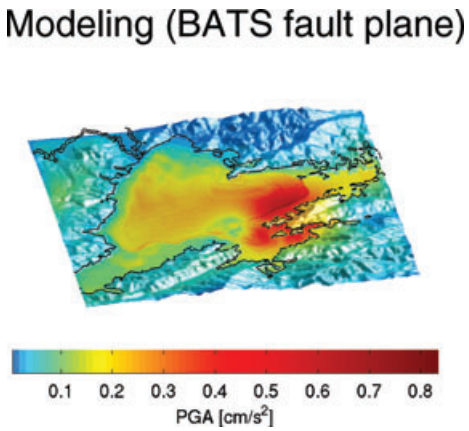

Figure 9. Simulated PGA distribution of the 2004 earthquake (fault plane after the BATS catalogue).

simulations indicates that fault orientation and movement have an important effect on resulting ground motions for the studied low frequency part for nearby earthquakes. This is consistent with findings from several studies of observed data which found that fault orientation can be found in the data in the low frequency part ($f <$ 0.5–4 Hz) for hypocentral distances of some tens of km (e.g. Vidale 1989; Takenaka *et al.* 2003; Castro *et al.* 2006).

5.3 Influence of the Sungshan formation

The Sungshan formation with its very low shear wave speeds (about 90–200 m s^{-1}) is a very distinct feature of the Taipei basin. The thickness of this uppermost soil layer varies between 50 m in the eastern part of the basin and 100 m in the NW of the basin. In this section, we evaluate the influence of this uppermost layer on ground motions. First, we simulate wave propagation for a model without Sungshan formation. Second, we apply a more detailed model of the Sungshan formation compared to the model applied in Sections 5.1 and 5.2. For both simulations we apply the fault plane solution published by Lee *et al.* (2006) because it seems to be the better one (see Section 5.2).

For the model without Sungshan formation, we apply eq. (2) so that the minimum surface shear wave velocity at the surface is equal to the minimum velocity of 450 m s^{-1} of the deeper sedimentary layers. The resulting PGA distribution is shown in Fig. 10. The shape of the distribution is similar to the distribution obtained from the calculation with the Sungshan formation (see Fig. 7). However, PGA is reduced by about 50 per cent. In Fig. 11 velocity seismograms are compared for both simulations. It can be seen that the inclusion of the Sungshan formation yields to an increase of maximum amplitude. Additionally, duration of ground shaking is longer for the model with Sungshan formation. This can be attributed to the generation and trapping of surface waves in the Sungshan formation. In order to explore the frequency characteristics, we evaluate spectral amplitudes for both models. Fig. 12 shows normalized spectral amplitudes for 0.25, 0.5, 0.75 and 1 Hz. The amplitudes are normalized to the maximum values for each frequency. The factor displayed in between the figures gives the amplification factor between the maxima of the simulations without and with Sungshan formation. It can

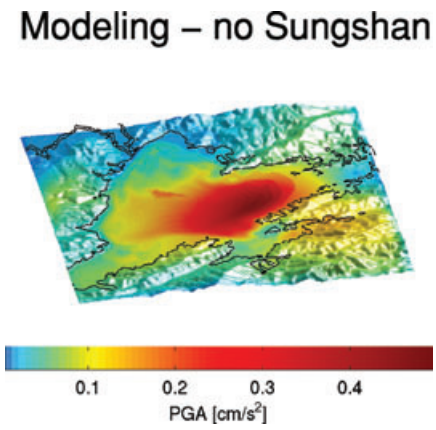

Figure 10. PGA distribution of the simulation for the model without Sungshan formation.

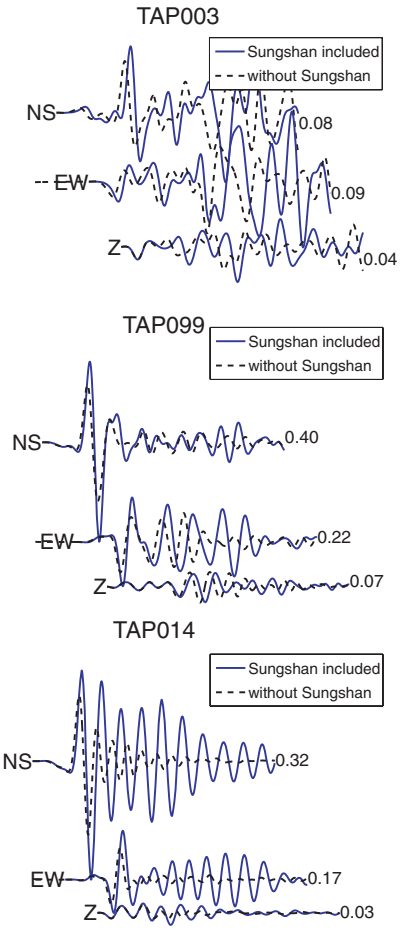

Figure 11. Seismograms for the simulations for the models with and without Sungshan formation.

be seen that for 0.25 and 0.5 Hz the distribution of spectral amplitudes is very similar for both models. Therefore, the deep basin structure controls the ground motion frequency content for both cases and the Sungshan formation amplifies the amplitudes by a factor of about 1.6 and 1.9, respectively. For 0.75 and 1 Hz differences in the distribution of spectral amplitudes are visible. Whereas for the simulation with Sungshan the areas of large amplitudes are shifted to the basin edges this effect cannot be seen for 0.75 Hz for the simulation without Sungshan. Only at 1 Hz large amplitudes occur also predominantly near the basin edge for the simulation without Sungshan. However, for the simulation with Sungshan formation this effect is seen more clearly. Consequently, the spectral values for 0.75 and 1 Hz for the model that contains the Sungshan formation can be explained by combined influence of the deep basin structure and the uppermost soft soil layer.

The above applied subsurface model is based on the average seismic velocities of the sedimentary layers given by (Wang *et al.* 2004) with constant minimum shear wave velocity at the surface of 170 m s^{-1}. There is also a more realistic model of the uppermost layers (down to a depth of 100 m) available which was also published by Wang *et al.* (2004). Fig. 13 displays the shear wave velocities of the Sungshan at the surface of this detailed model. In this model the surface shear wave velocities vary between 90 and 200 m s^{-1}. For this model maximum frequency of our FD simulations is 0.5 Hz because of the lower minimum shear wave velocities of about 90 m s^{-1} compared to 170 m s^{-1} for our previous models. The resulting PGA for frequencies lower than 0.5 Hz are shown in Fig. 14 for frequency smaller than 0.5 Hz for the detailed and simplified Sungshan formation. There is almost no difference visible between both PGA distributions. Also the waveforms are very similar (Fig. 15). This suggests that for low frequency ground motion simulation the application of the simplified Sungshan structure with constant surface velocities is sufficient. This minor influence of the locally very small surface shear wave velocities was also found by Day *et al.* (2008) for ground motion simulations for southern California.

5.4 Influence of earthquake location

The distribution of normalized spectral amplitudes shown in Fig. 12 for 0.75 and 1 Hz show that large amplitudes are obtained in the part of the basin that is near the epicentre location (see Fig. 3). This raises the question how strong the obtained distribution of spectral values depends on epicentre location. From the Los Angeles basin the dependence of site effects on earthquake location is well known (Field & the SCEC Phase III Working Group 2000; Hruby & Beresnev 2003). To explore the strength of dependence of spectral amplifications on earthquake azimuth for the Taipei basin, we simulate a scenario earthquake in the southwestern corner of the Taipei basin. The new location is also shown in Fig. 3. We rotated the strike of this earthquake to 285° so that large *S*-wave amplitudes are radiated into the basin like in the case of the real 2004 earthquake. Depth, dip and rake of this scenario earthquake are the same as for the 2004 event. As both events radiate large *S*-wave amplitudes into the basin the resulting spectral amplifications do not depend strongly on source radiation. Therefore, resulting spectral amplifications show mainly the influence of earthquake azimuth. By doing so we do not consider the path effect, which is assumed to be small because of the relatively smooth subsurface structure beneath the Taipei basin. In Fig. 16 spectral amplitudes are shown for the scenario event. The strong influence of epicentre location is clearly visible. The distribution not only changes for 0.75 and 1 Hz but also for 0.25 and 0.5 Hz. For the low frequencies largest spectral amplitudes are found in the deep western part of the basin. For example the area of large amplitudes for the real 2004 earthquake in the eastern part of the basin does not occur for the scenario earthquake. And as in the case of the 2004 earthquake the areas of larger amplitudes for 0.75 and 1 Hz occur in the SW in the direction of the epicentre. Therefore, we conclude that spectral amplitudes strongly depend on earthquake azimuth.

When comparing our findings with H/V ratios obtained from observed earthquakes at TSMIP stations within the basin, we can see the same general effect. Fig. 17 shows H/V ratios obtained from recorded earthquakes of the TSMIP network (Wen & Peng 1998; Wen *et al.* 2007). For 0.5 Hz mainly the eastern and deep western part of the basin show large spectral amplitudes. The observed distribution seems to be a combination of the spectral amplitude distributions of the two modelled earthquakes (see Figs 12 and 16). This is reasonable because the observed H/V values are based on earthquakes that occur mainly from azimuths between East and Southwest and consequently the resulting distribution of spectral amplification reflects an average over all azimuths. Our analysis is based on the simulation of two near-field earthquakes. As described above, by rotating the strike of the scenario earthquake maximum amplitudes, which are radiated into the basin, are similar to the real 2004 event. Therefore, differences in PGA and spectral amplifications do not depend on the underlying source mechanism but

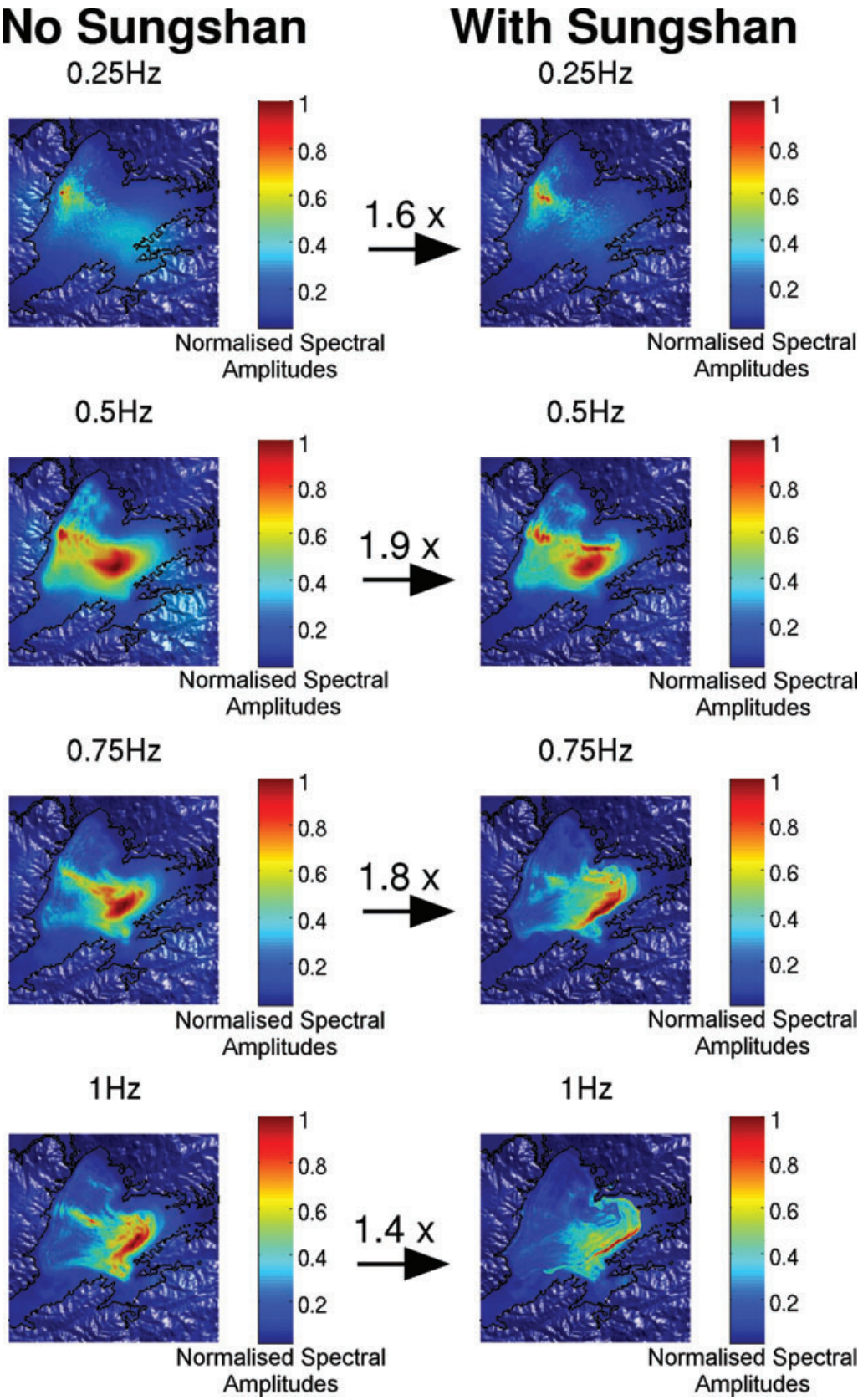

Figure 12. Distribution of normalized spectral amplitudes for the models with and without Sungshan formation. The numbers in between the figures give the amplification factors of the maximum values of the simulation with Sungshan compared to the simulation without Sungshan.

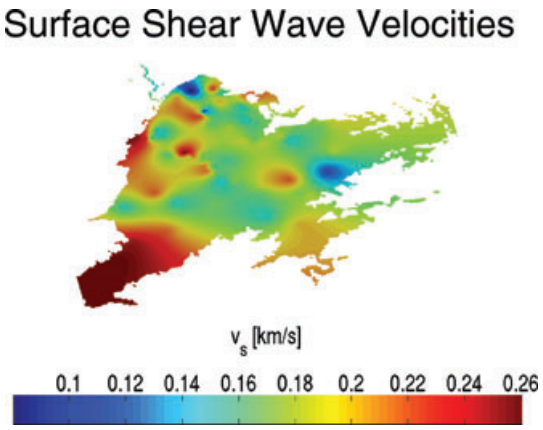

Figure 13. Surface shear wave velocities of the realistic Sungshan model given by Wang *et al.* (2004).

only on earthquake azimuth and basin structure. However, future simulations for earthquakes of different azimuths, depths, distances and radiation patterns are recommended in order to analyse more accurately the influence of earthquake azimuth. Especially, as path effects for more distant events may become more important. However, our simple simulation shows that azimuthal effects may be very dominant, which is also supported by the above shown good comparison between simulated and observed spectral amplifications. This means that when looking at a particular scenario earthquake our simulation shows that the ground motion parameters may clearly differ from the obtained average distribution because of the strong azimuthal effects. Especially for possible strong earthquakes on the known faults close to the Taipei basin with predominant source mechanism hazard assessment based on the azimuthal averaged values could significantly underestimate future ground motion. Unfortunately, there is no map for observed spectral values at 1 Hz available. Therefore, we show here only the observed values for 2 Hz (Fig. 17). Maximum values occur close to the basin edges, which is the same trend as we can see in our calculated values for 1 Hz.

5.5 Spectral amplifications

Here, we simulate wave propagation for the 2004 earthquake in a model without the Taipei basin structure. The model only includes the 3-D structure of the region obtained from seismic tomography by Wu *et al.* (2007). The *P*- and *S*-wave velocities at the surface

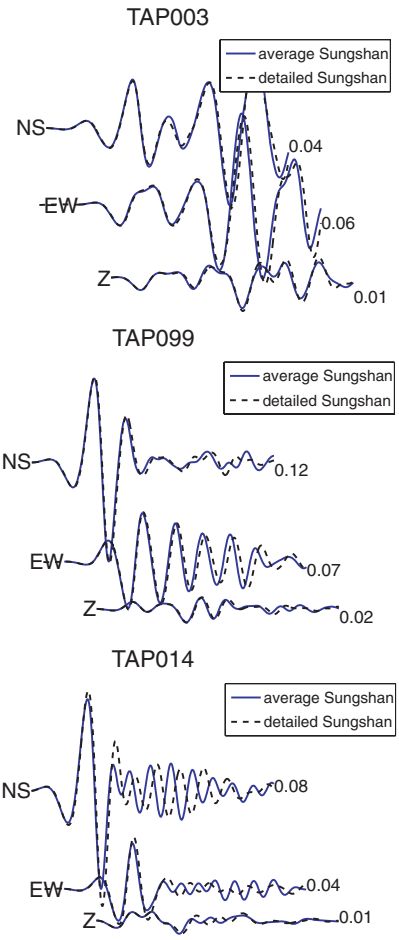

Figure 15. Velocity seismograms for the models with average Sungshan properties and the realistic Sungshan model.

vary from 2.59 to 5.72 km s^{-1} and 1.43 to 3.30 km s^{-1}, respectively. Consequently the simulation results reflect ground motion for hard rock conditions. We averaged the obtained spectral amplitudes for the area that corresponds to the basin area and use this as a reference spectrum. We calculated spectral ratios between the 2004 earthquake results (see Section 5.1) and the results obtained in this section. Fig. 18 shows the resulting spectral ratios for 0.5 Hz. We also calculated spectral ratios for the scenario earthquake in the SW (Fig. 19). Both simulations show maximum amplification

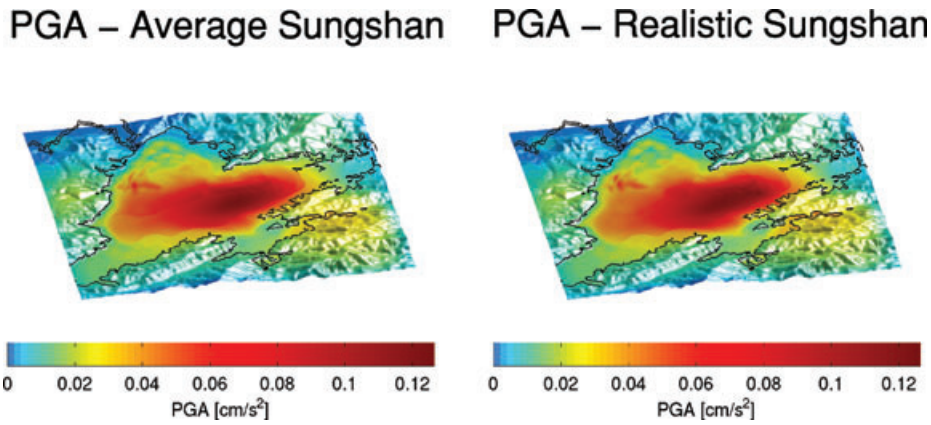

Figure 14. PGA distributions for the models with average Sungshan properties and the realistic Sungshan model for $f < 0.5$ Hz.

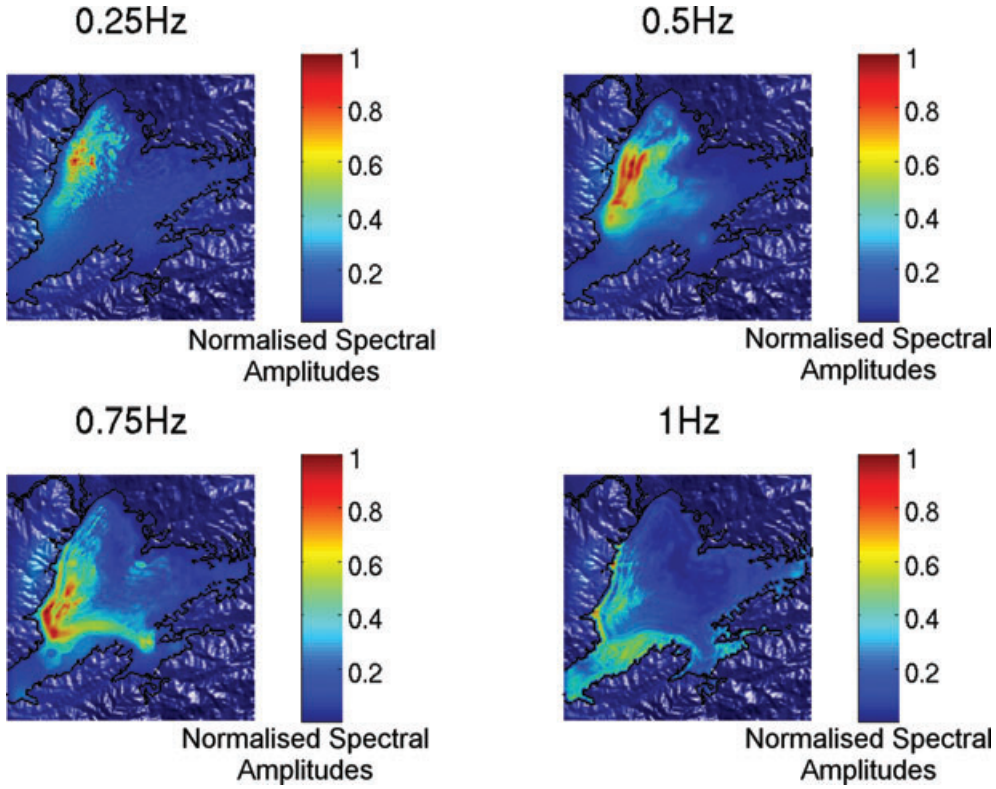

Figure 16. Normalized spectral amplitudes for the scenario earthquake near the SW basin edge.

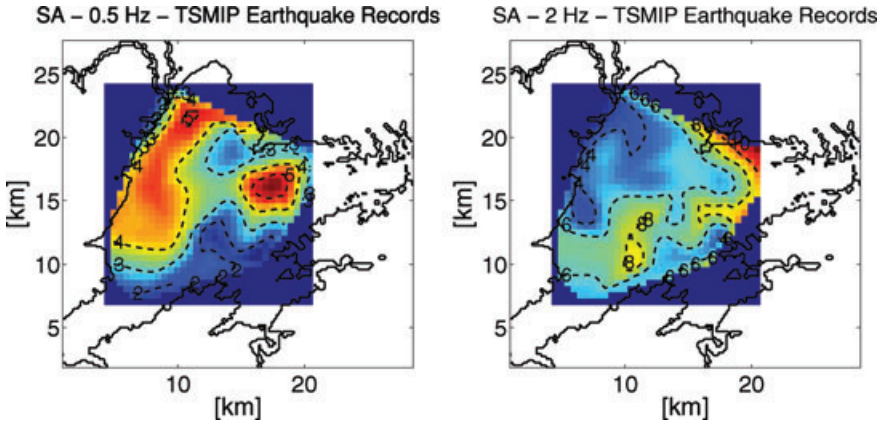

Figure 17. Spectral ratios obtained from TSMIP earthquake records of 0.5 and 2 Hz (Wen & Peng 1998).

factors of about 8–9. This is in good comparison with the values of more than five obtained from the empirical study (see Fig. 17). From this study, we can assess that the basin structure results in an amplification value of about 8. From our study of the influence of the Sungshan formation, we found that the Sungshan formation increases amplification by a factor of about 2. Therefore, we can give as an estimate an amplification factor of about 4 for the deep basin structure.

Finally we compare our amplification values with theoretical values calculated by considering the 1-D soil column beneath the stations. The low frequency part for such a study (Sokolov *et al.* 2009) is only available for seven stations in the western deep part of the basin. Fig. 20 compares the 1-D values with the amplification obtained from the 2004 earthquake and scenario modelling. In general the values obtained from our modelling are clearly larger than the 1-D results. 1-D amplification values vary between 2 and 3 whereas the amplifications from our study show values up to 7, which are consistent with the observed values in Fig. 17 after Wen *et al.* (2007) and Wen & Peng (1998). Exceptions are stations TAP 10 and TAP 12 where 1-D amplification values are larger than the values for the scenario earthquake in the SE because for this earthquake only the western deep part is affected by large ground motion. At station TAP 4 1-D amplification are larger than our obtained values for both earthquakes for frequencies larger than 0.5 Hz. This occurs because none of our simulated earthquake produced significant ground shaking in the northern tip of the Taipei basin. Our comparison shows that effects like surface waves generation, focusing, and influence of the 3-D structure are very important and necessary because they produce amplification values that are up to three times larger compared to the calculated 1-D effects.

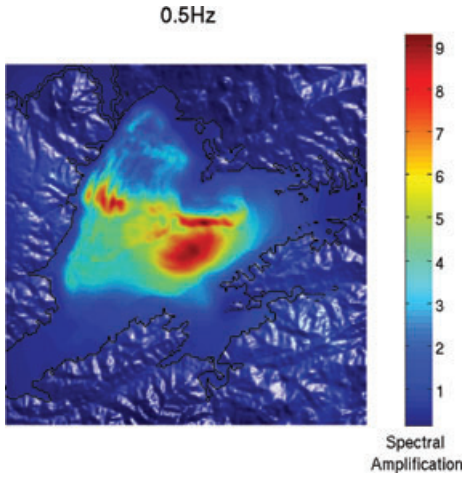

Figure 18. Spectral amplifications with respect to the model without basin structure for the 2004 earthquake.

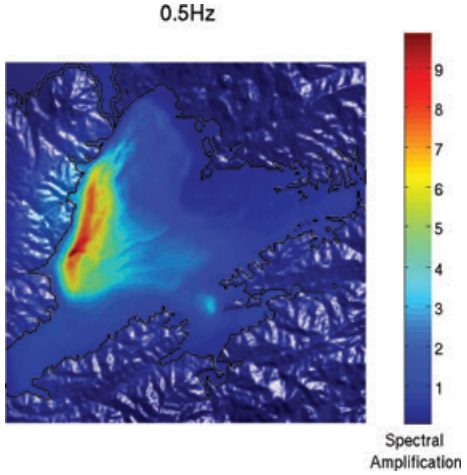

Figure 19. Spectral amplifications with respect to the model without basin structure for the scenario earthquake.

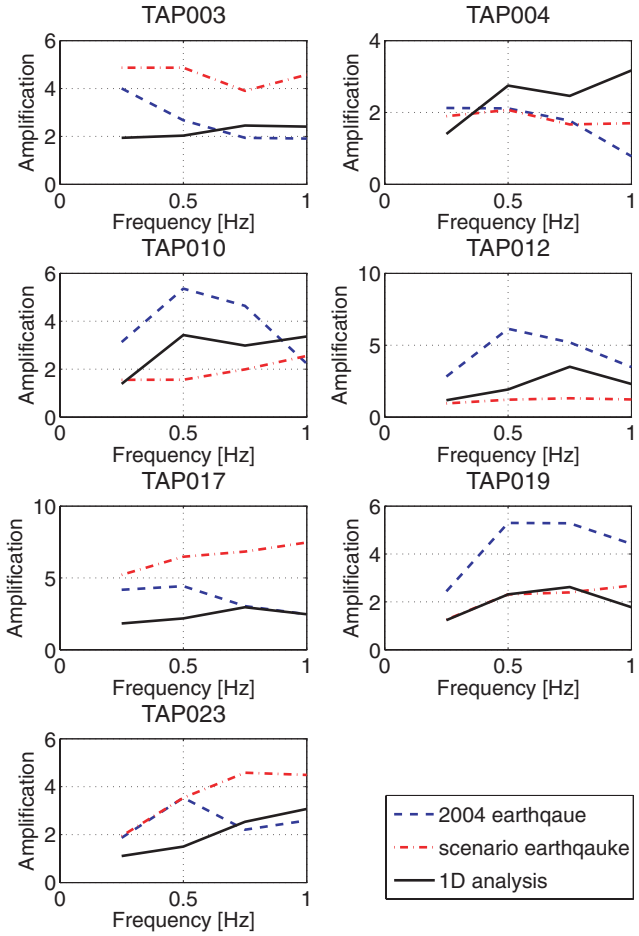

Figure 20. Comparison of spectral amplifications of the 2004 and scenario earthquake with theoretical 1-D amplification values after Sokolov *et al.* (2009) for seven stations in the western deep part of the basin.

6 DISCUSSION AND CONCLUSIONS

In this study we used a $M_L = 3.8$ earthquake that occurred in the vicinity of the Taipei basin as a testing case to calculate ground motions and to evaluate the influence of source and basin effects on the resulting ground motion. Wave propagation was simulated by a 3-D FD method (Furumura & Kennett 2005). Based on high quality data, we were able to build a 3-D model that incorporates recent research results on the Taipei basin structure (Wang *et al.* 2004) and the crustal and mantle structure of Taiwan (Wu *et al.* 2007). It was not possible to include surface topography in the applied FD scheme. However, topography can have influence on ground motions in the Taipei basin as shown by Lee *et al.* (2009). On the other hand these effects seems to be most important for distant earthquakes due to the mountain ranges on the wave path. Therefore, such topographic effect may have little influence for local earthquakes.

From the comparison of modelling and observation, we found that our simulation results reproduced the observed horizontal waveforms for stations clearly within the basin and the observed PGA distribution of the 2004 October 23 event. Only for stations near the basin edges the waveforms differed. However, maximum amplitudes were reproduced by the modelling in most cases. In general, large differences in waveforms were found for the vertical components. This may be a general problem of modelling or observed data as the numerical simulation by a SEM done by Lee *et al.* (2008b) also produced larger misfits of the vertical components compared to the horizontal ones. However, maximum amplitudes of the vertical component were reproduced by both modelling schemes. In summary, our study suggests that the created 3-D subsurface model and the applied 3-D FD method are appropriate to simulate ground motions for the Taipei basin.

We compared ground motions of two different published fault plane orientations. The first one is based on Lee *et al.* (2006). The second one is a quick CMT solution, which was taken from the BATS catalogue. We found that the solution of Lee *et al.* (2006) showed a significantly better fit between observation and modelling compared to the BATS solution. Consequently, when looking at low frequency ground motions for earthquakes the fault plane parameters are critical. This is the case at least for earthquakes in the vicinity of the Taipei basin.

Next we analysed the influence of the low velocity Sungshan formation by comparing our simulation results with a simulation for a model that does not contain this low velocity surface layer. We found that the Sungshan formation amplifies PGA and peak spectral amplitudes by a factor of about two. However, only minor changes in the frequency content of the signals were obtained. As the real Sungshan formation is more complex we compared our

simulation for a constant surface velocity of 170 m s^{-1} with simulation results for the more realistic surface velocity distribution between 90 and 200 m s^{-1} for frequencies lower than 0.5 Hz. Here we found that the more realistic structure of the Sungshan formation has negligible influence compared to the use of the average properties of the Sungshan formation. This suggests that the application of the model described in Section 2 is appropriate for low frequency ground motion simulations. However, this should be also evaluated by computational more costly calculations up to 1 Hz. We found that mainly the deep basin structure influences the distribution of spectral values for frequencies lower than about 0.5 Hz. For larger frequencies both the deep basin structure as well as the uppermost Sungshan formation influence the distribution of spectral values.

Our analysis of spectral amplification factors showed that the basin structure produces amplification values of about 4. With amplifications due the soft soil Sungshan formation of about 2, total amplification is around 8, which is in good comparison with analysis of observed data. Furthermore, we found that the two dominant regions of large spectral amplifications in the eastern shallow part and in the western deep part obtained from empirical data can be explained by azimuthal effects. Earthquakes in the SE produce larger amplifications in the eastern part of the basin and earthquakes in the SW generate strong shaking in the western deep part.

This study showed the reliability of the applied 3-D FD method and of the created 3-D subsurface structure of the Taipei basin area. Therefore, simulations of potential large earthquakes that may occur near the basin can be performed in future. From our study, we found that earthquake location and fault plane solution of potential future earthquakes close to the Taipei basin are very critical parameters. Therefore, numerical modelling of future ground motions from earthquakes on localized faults near the Taipei basin is of high priority, as hazard assessment based on averaged values over all earthquake azimuths, which are obtained from empirical data, may significantly underestimate future ground motions.

ACKNOWLEDGMENTS

We thank Takashi Furumura for providing the 3-D finite-difference code. We are grateful to Chien-Ying Wang for the Taipei basin model and to Yih-Min Wu for providing the seismic tomography results. The simulations were performed on a HPXC6000 system of the Scientific Supercomputing Center Karlsruhe. This work was funded by the Deutsche Forschungsgemeinschaft, Germany (DFG - project WE 1394/13-1 and MI 1375/2-1) and the National Science Council, Taiwan, ROC (grant NSC 96-2119-M-008-007). We also thank two anonymous reviewers for their valuable comments and suggestions.

REFERENCES

Blanch, J.O., Robertsson, J.O.A. & Symes, W.W., 1995. Modeling of a constant Q: methodology and algorithm for an efficient and optimally inexpensive viscoelastic technique, *Geophysics,* **60**(1), 176–184.

Castro, R.R., Franceschina, G., Pacor, F., Bindi, D. & Luzi, L., 2006. Analysis of the frequency dependence of the S-wave radiation pattern from local earthquakes in central Italy, *Bull. seism. Soc. Am.,* **96**(2), 415–426.

Cerjan, C., Kosloff, D., Kosloff, R. & Reshef, M., 1985. A nonreflecting boundary condition for discrete and elastic wave equations, *Geophysics,* **50**(4), 705–708.

Chen, K.-C., 2003. Strong ground motion and damage in the Taipei basin from the Moho reflected seismic waves during the March 31, 2002, Hualien, Taiwan earthquake, *Geophys. Res. Lett.,* **30**(11), 1551.

CIAT, 2004. Void-filled seamless SRTM data v1, 2004, International Centre for Tropical Agriculture (CIAT), available from the CGIAR-CSI SRTM 90m Database: http://srtm.csi.cgiar.org.

Clayton, R. & Enquist, B., 1977. Absorbing boundary conditions for acoustic and elastic wave equations, *Bull. seism. Soc. Am.,* **67**(6), 1529–1540.

Day, S., Graves, R., Bielak, J., Dreger, D., Larsen, S., Olsen, K., Pitarka, A. & Ramirez-Guzman, L., 2008. Model for basin effects on long-period response spectra in southern California, *Earthq. Spectra,* **24,** 257–277.

Field, E.H. & the SCEC Phase III Working Group, 2000. Accounting for site effects in probabilistic seismic hazard analyses of southern California: overview of the SCEC phase III report, *Bull. seism. Soc. Am.,* **90**(6B), S1–31.

Fletcher, J.B. & Wen, K.-L., 2005. Strong ground motion in the Taipei basin from the 1999 Chi-Chi, Taiwan, earthquake, *Bull. seism. Soc. Am.,* **95**(4), 1428–1446.

Furumura, T. & Chen, L., 2004. Large scale parallel simulation and visualization of 3-D seismic wavefield using the Earth Simulator, *Comput. Model. Eng. Sci.,* **6**(2), 153–168.

Furumura, T. & Chen, L., 2005. Parallel simulation of strong ground motions during recent and historical damaging earthquakes in Tokyo, Japan, *Parallel Comput.,* **31**(2), 149–165.

Furumura, T. & Kennett, K., 2005. Subduction zone guided waves and the heterogeneity structure of the subducted plate: intensity anomalies in northern Japan, *J. geophys. Res.,* **110,** B10302, doi:10.1029/2004JB003468.

Glaznev, V.N., Raevsky, A.B. & Skopenko, G.B., 1996. A three-dimensional integrated density and thermal model of the Fennoscandian lithosphere, *Tectonophysics,* **258,** 15–33.

Graves, R.W., 1996. Simulating seismic wave propagation in 3D elastic media using staggered-grid finite differences, *Bull. seism. Soc. Am.,* **86**(4), 1091–1106.

Hruby, C.E. & Beresnev, I.A., 2003. Empirical corrections for basin effects in stochastic ground-motion prediction, based on the Los Angeles basin analysis, *Bull. seism. Soc. Am.,* **93**(4), 1679–1690.

Kristeková, M., Kristek, J. & Moczo, P., 2009. Time-frequency misfit and goodness-of-fit criteria for quantitative comparison of time signals, *Geophys. J. Int.,* **178**(2), 813–825.

Lee, S.J., Huang, B.S. & Liang, W.T., 2006. Grid-based moment tensor inversion by using spectral-element method 3D Green's functions, in West. Pac. Geophys. Meet. Suppl., vol. EOS 87(36), Abstract S11C-0137.

Lee, S.-J., Chen, H.-W. & Huang, B.-S., 2008a. Simulations of strong ground motion and 3D amplification effect in the Taipei basin by using a composite grid finite-difference method, *Bull. seism. Soc. Am.,* **98**(3), 1229–1242.

Lee, S.-J., Chen, H.-W., Liu, Q., Komatitsch, D., Huang, B.-S. & Tromp, J., 2008b. Three-dimensional simulations of seismic-wave propagation in the Taipei basin with realistic topography based upon the spectral-element method, *Bull. seism. Soc. Am.,* **98**(1), 253–264.

Lee, S.-J., Chan, Y.-C., Komatitsch, D., Huang, B.-S. & Tromp, J., 2009. Effects of realistic surface topography on seismic ground motion in the Yangminshan region of Taiwan based upon the spectral-element method and LiDAR DTM, *Bull. seism. Soc. Am.,* **99**(2A), 681–693.

Lin, P.-S. & Lee, C.-T., 2008. Ground-motion attenuation relationships for subduction-zone earthquakes in northeastern Taiwan, *Bull. seism. Soc. Am.,* **98**(1), 220–240.

Madariaga, R., 1976. Dynamics of an expanding circular fault, *Bull. seism. Soc. Am.,* **66**(1), 639–666.

Miksat, J., Müller, T. & Wenzel, F., 2008. Simulating 3D seismograms in 2.5D structures by combining 2D finite-difference modeling and ray tracing, *Geophys. J. Int.,* **174**(1), 309–315.

Miksat, J., Wen, K.-L., Chen, C.-T., Sokolov, V. & Wenzel, F., 2009. Simulating the Taipei basin response by numerical modeling of wave propagation, *Bull. Earthq. Eng.,* **8**(4), 847–858, doi:10.1007/S10518-009-9171-0.

Moczo, P., Kristek, J., Vavrycuk, V., Archuleta, R.J. & Halada, L., 2002. 3D heterogeneous staggered-grid finite-difference modeling of seismic motion with volume harmonic and arithmetic averaging of elastic moduli and densities, *Bull. seism. Soc. Am.,* **92**(8), 3042–3066.

Olsen, K.B., Akinci, A., Rovelli, A., Marra, F. & Malagnini, L., 2006. 3D ground-motion estimation in Rome, Italy, *Bull. seism. Soc. Am.,* **96**(1), 133–146.

Sokolov, V., Wen, K.-L., Miksat, J., Wenzel, F. & Chen, C.-T., 2009. Analysis of Taipei basin response on earthquakes of various depth and location using empirical data, *Terr. Atmos. Ocean. Sci,* **20**(5), 687–702, doi:10.3319/TAO.2008.10.15.01(T).

Sokolov, V.Y., Loh, C.-H. & Wen, K.-L., 2000. Empirical study of sediment-filled basin response: the case of Taipei city, *Earthq. Spectra,* **16**(3), 681–707.

Sokolov, V.Y., Loh, C.-H.&Wen, K.-L., 2003. Evaluation of hard rock spectral models for the Taiwan region on the basis of the 1999 Chi-Chi earthquake data, *Soil Dyn. Earthq. Eng.,* **23**(8), 715–735.

Sokolov, V.Y., Loh, C.-H. & Wen, K.-L., 2004. Evaluation of generalized site response functions for typical soil classes (B, C, and D) in Taiwan, *Earthq. Spectra,* **20**(4), 1279–1316.

Takenaka, H., Mamada, Y. & Futamure, H., 2003. Near-source effect on radiaton pattern of high-frequency S waves: strong SH-SV mixing observed from aftershocks of the 1997 Northwestern Kagoshima, Japan earthquakes, *Phys. Earth. planet. Int.,* **137,** 31–43.

Teng, L.S., Lee, C.T., Peng, C.-H., Chen, W.-F. & Chu, C.-J., 2001. Origin and geological evolution of the Taipei basin, northern Taiwan, *Western Pacific Earth Sci.,* **1**(2), 115–142.

Vidale, J.E., 1989. Influence of focal mechanism on peak accelerations of strong motions of the Whittier Narrows, California, earthquake and an aftershock, *J. geophys. Res.,* **94**(B7), 9607–9613.

Wang, C.Y., Lee, Y.-H., Ger, M.-L. & Chen, Y.-L., 2004. Investigating subsurface structures and P- and S-wave velocities in the Taipei Basin, *Terr. Atmos. Ocean. Sci,* **15**(4), 609–627.

Wen, K.-L. & Peng, H.-Y., 1998. Site effect analysis in the Taipei basin: results from TSMIP network data, *Terr. Atmos. Ocean. Sci,* **9**(4), 691–704.

Wen, K.-L., Lin, C.-M. & Chen, C.-T., 2007. Site response in the Taipei urban area from dense microtremor survey, in *Fourth International Conference on Urban Earthquake Engineering*, Center for Urban Earthquake Engineering, Tokyo Institute of Technology, Tokyo, Japan, 5–6 March, pp. 139–146.

Wu, Y., Chang, C., Zhao, L., Shyu, J., Chen, Y., Sieh, K. & Avouac, J., 2007. Seismic tomography of Taiwan: improved constraints from a dense network of strong motion stations, *J. geophys. Res,* **112**, B08312, doi:10.1029/2007JB004983.